Two-step regulation of centromere distribution by condensin II and the nuclear envelope proteins

Takuya Sakamoto
Yuki Sakamoto
Osaka University
Stefan Grob
University of Zurich
Tomoe Yamashita
Tokyo University of Science
Nanami Ito
Tokyo University of Science
Yuka Oko
Tokyo University of Science
Tomoya Sugiyama
Tokyo University of Science
Takumi Higaki
Kumamoto University
Seiichiro Hasezawa
Graduate School of Science and Engineering, Hosei University
Maho Tanaka
RIKEN Center for Sustainable Resource Science
Akihiro Matsui
RIKEN Center for Sustainable Resource Science
Motoaki Seki
RIKEN Center for Sustainable Resource Science https://orcid.org/0000-0001-8288-0467
Takamasa Suzuki
Chubu University
Ueli Grossniklaus
University of Zurich https://orcid.org/0000-0002-0522-8974
Sachihiro Matsunaga (sachi@edu.k.u-tokyo.ac.jp)
University of Tokyo https://orcid.org/0000-0003-3024-3559

Article

Keywords: centromere distribution, genome integrity, Arabidopsis thaliana, condensin II, linker of the nucleoskeleton and cytoskeleton (LINC)

Posted Date: September 30th, 2021

DOI: https://doi.org/10.21203/rs.3.rs-793150/v1

Version of Record: A version of this preprint was published at Nature Plants on August 1st, 2022. See the published version at https://doi.org/10.1038/s41477-022-01200-3.

Abstract

The arrangement of centromeres within the nucleus differs among species and cell types. However, neither the mechanisms determining centromere distribution nor its biological significance are currently well understood. In this study, we demonstrate the importance of centromere distribution for the maintenance of genome integrity through the cytogenic and molecular analysis of mutants defective in centromere distribution. We propose a two-step regulatory mechanism that shapes the non-Rabl-like centromere distribution in *Arabidopsis thaliana* through condensin II and the linker of the nucleoskeleton and cytoskeleton (LINC) complex. Condensin II is enriched at centromeres and, in cooperation with the LINC complex, induces the scattering of centromeres around the nuclear periphery during late anaphase/telophase. Then, after entering interphase, the positions of the scattered centromeres are stabilized by nuclear lamina proteins of the CROWDED NUCLEI (CRWN) family. We also found that, despite their strong impact on centromere distribution, condensin II and CRWNs have little effect on chromatin organization involved in the control of gene expression, indicating the robustness of chromatin organization regardless of the type of centromere distribution.

Introduction

The centromere is a constitutive heterochromatic domain that is universally conserved in all eukaryotic chromosomes. The spatial arrangement of centromeres within the nuclear space in mitotic interphase differs among species, cell type, cell cycle stage, and differentiation state[1–3]. Centromere distribution is classified into two types: Rabl and non-Rabl configurations[1–4]. In the Rabl configuration, the centromeres are grouped at one side of the nucleus, whereas the telomeres, constituting another universal constitutive heterochromatic domain, are clustered in the opposite nuclear hemisphere. Contrastingly, in non-Rabl configuration, the centromeres and telomeres are uniformly dispersed within the nucleus[5]. The Rabl configuration can be considered the ‘default’ organization of interphase chromatin, as it retains the orientation of chromosomes that segregate during anaphase[3]. Therefore, mechanisms acting after anaphase are required to establish a non-Rabl centromere configuration[6]; however, the underlying processes are yet to be fully understood.

In *Arabidopsis thaliana*, the centromeres are scattered in the nucleus near the nuclear periphery, adopting a non-Rabl configuration[7,8]. Condensin II, composed of two structural maintenance of chromosome (SMC) proteins and three non-SMC proteins (CAP-D3, CAP-G2, and CAP-H2), is required to prevent the hyperclustering of centromeres[9,10]. Among the CROWDED NUCLEI (CRWN) proteins that form a meshwork structure at the nuclear lamina[11], CRWN1, CRWN2, and CRWN4 function in the unclustering of chromocenters, which are densely compacted heterochromatic regions containing centromeric and pericentromeric DNA[11–14]. In addition, CRWN1 directly interacts with heterochromatin, including the centromeric and pericentromeric regions[15]. The Sad1/UNC-84 (SUN) domain proteins, subunits of the linker of the nucleoskeleton and cytoskeleton (LINC) complex, are involved in maintaining the centromeres near the nuclear periphery[13]. However, the role of these factors in establishing interphase

centromere distribution is not well understood. Moreover, although these factors play similar roles in the spatial arrangement of centromeres, whether they function in a coordinated and concerted manner remains unclear.

In this study, we demonstrate the concerted action of condensin II and the LINC complex to determine centromere distribution during mitosis. In addition, we found that CRWN1 and CRWN4 are required to stabilise centromere distribution during interphase. Our work reveals a coordinated mechanism consisting of two steps that enables non-Rabl-type centromere distribution. Moreover, the characterisation of mutants affecting centromere distribution revealed a role of centromere configuration in maintaining genome integrity but not chromatin organization, which is associated with regulating gene expression.

Results

Condensin II is enriched at centromeres from late G2 through early G1 phase

To further characterise the function of condensin II, its subnuclear localisation was investigated using GFP fused to CAP-G2, a subunit specific to condensin II in wild-type *Arabidopsis* nuclei. Because condensin II is strongly expressed in root tips[16], we studied cells in the meristematic, elongating, and differentiated zones of the root. In all regions, GFP-tagged condensin II signals were detected in both the nucleoplasm and nucleolus (Fig. 1a). A similar subnuclear localisation was observed in tobacco BY-2 cells expressing *Arabidopsis* CAP-H2-GFP[17]. Moreover, we found that some nuclei showed a spot-like localisation of condensin II only in the meristematic zone, in addition to its basic localisation throughout the nucleus (Fig. 1a and Supplementary Fig. S1). Given that the cells in the meristematic zone proliferate, it is possible that the formation of a spot-like localisation of condensin II is cell cycle-dependent. Indeed, using time-lapse imaging analysis of GFP-tagged condensin II during the mitotic cell cycle, the spot-like localisation of condensin II was observed 80 min prior to metaphase and disappeared around 40 min after metaphase, corresponding to late G2 and early G1 phase, respectively (Fig. 1b).

In the primitive red alga *Cyanidioschyzon merolae* and in the nematode *Caenorhabditis elegans*, condensin II is specifically localised to centromeres from prophase through anaphase[18,19]. Thus, we hypothesised that the condensin II spots in *A. thaliana* nuclei colocalize with centromeres. Ideally, mitotic cells display 10 discrete centromere signals, which can be visualised by fluorescent fusion protein tdTomato-CENH3 (centromeric histone H3). As expected, our observations revealed that each CAP-G2-GFP signal colocalized with a tdTomato-CENH3 signal (Fig. 1c). Collectively, these results suggest that condensin II accumulates at centromeres during this specific cell cycle phase.

Condensin II is required for scattering centromeres in telophase

Fluorescent *in situ* hybridization (FISH) analysis has shown that condensin II is indispensable for the dissociation of centromeres in interphase nuclei[9,10]. To determine how condensin II participates in the dynamic regulation of centromeres during the cell cycle, we conducted live imaging of tdTomato-CENH3

in the *cap-h2-2*[16] null mutant. Contrary to the scattered centromere distribution in the wild type, the *cap-h2-2* mutant showed a biased centromere distribution, in which almost all centromeres were clustered at one side of the nucleus. This occurred not only in meristematic cells, but also in differentiated cells of the root (Fig. 2a). Then, we quantitatively evaluated the degree of bias in centromere distribution. Given that cells above the stem cell niche divide longitudinally into the root apical meristem, we determined an equatorial plane that produces two hemispheres in the nucleus using the centre points of two nuclei neighbouring the target nucleus in the same cell file. We calculated the degree of bias in centromere distribution by counting the number of centromeres in each hemisphere (Fig. 2b, left panel). The *cap-h2-2* mutant showed an extremely biased centromere distribution compared to the wild type (Fig. 2b, right panel).

To determine the period during which centromere positioning mediated by condensin II was established, we monitored centromere dynamics from anaphase to early G1 phase (Fig. 2c). In the wild type, all centromere pairs were aligned along the metaphase plate. Then, sister centromeres moved to opposite poles in anaphase, subsequently scattering in telophase (Fig. 2c)[7,20]. Our imaging analysis revealed that during the transition from anaphase to telophase, the centromeres remained at opposite poles in the *cap-h2-2* mutant (2.5 to 7.5 min in Figure 2c). This position persisted after entry into G1 phase (25 and 45 min in Fig. 2c). Given that condensin II was localised to centromeres throughout mitosis (Fig. 1), condensin II function at centromeres during the transition from anaphase to telophase seems indispensable for centromere scattering.

Nuclear envelope-related factors are involved in scattering centromeres in cooperation with condensin II

Nuclear envelope (NE) reassembly occurs in plants during the transition from anaphase to telophase during mitosis[20,21]. In *Arabidopsis*, at late anaphase, the NE proteins SUN1 and SUN2 are reassembled at the distal surfaces of the chromosomes, where centromeres are found. These proteins enclose the chromosomes from the distal surface to the proximal surface at telophase[20,20]. Similar dynamics have been observed for plant nuclear lamina proteins, namely nuclear matrix constituent proteins (NMCPs), in *Apium graveolens* (celery)[21]. Because the timing between the reassembling of NE-related factors and centromere scattering is approximately the same, we hypothesised that NE-related factors are involved in centromere scattering.

The SUNs (SUN1-SUN5) are inner nuclear membrane proteins comprising the LINC complex in association with other proteins[22]. SUNs have the potential to interact with chromatin in the nucleoplasm, along with their interactions with Klarsicht/ANC-1/Syne homology (KASH)-domain proteins, such as WPP domain-interacting proteins (WIPs) and SUN-interacting NE proteins (SINEs) in the outer nuclear membrane. Through interactions between KASH or KASH-associated proteins, such as WPP domain-interacting tail-anchored proteins (WITs) and myosin XI-I, with actin filaments, the SUNs are also connected to the cytoskeleton[22]. The nuclear lamina comprising *Arabidopsis* NMCPs, known as CRWN proteins, is located underneath the NE (Fig. 3a)[22,23]. To evaluate the involvement of NE-related factors in centromere scattering, we analysed centromere distribution in mutants affecting the LINC complex and

CRWN proteins (Fig. 3b–e). Mutants affecting KASH (*wifi* and *sine1-1*) and SUN proteins (*sun1-KOsun2-KD* and *sun4sun5*) showed a significantly more biased centromere distribution than the wild type, although the bias was not as pronounced as previously observed in the condensin II mutant. In contrast, centromere distribution in the *crwn1crwn4* and *myosin xi-i* mutants was comparable to that in the wild type (Fig. 3b,c). Additionally, we found that the inhibition of actin polymerisation by latrunculin B treatment caused a biased centromere distribution, while treatment with oryzalin, resulting in microtubule depolymerisation, did not affect it (Fig. 3d,e). These results suggest that, in addition to condensin II, the LINC complex associated with actin filaments is involved in determining centromere distribution during mitosis.

Next, we investigated whether the LINC complex associates with the centromere and/or condensin II to regulate centromere distribution. Among LINC complex components, only the SUNs have the potential to interact with chromatin as a part of the SUN domain in the nucleoplasm[22]. Therefore, we evaluated the interaction of SUN proteins with CENH3 and condensin II by co-immunoprecipitation (co-IP). Our co-IP analyses after transient expression of the proteins in tobacco leaves indicated interactions of SUN1 and SUN2 with CENH3 (Fig. 3f). Similarly, we found an interaction between SUN2 and the condensin II component CAP-G2 using co-IP assays (Fig. 3g). The interactions between the SUNs and condensin II components were further supported by yeast two-hybrid assays (Fig. 3h) and bimolecular fluorescence complementation (Bi-FC) assays in cultured tobacco BY-2 cells (Supplementary Fig. 2). Collectively, these results suggest that the LINC complex is essential for correct centromere distribution in interphase through interactions between SUNs, centromeres, and condensin II, most likely during the transition from anaphase to telophase. The corresponding mutants did not show a marked alteration in centromere distribution, as was observed in *cap-h2-2,* suggesting functional redundancy among SUN and KASH proteins. Hereafter, we termed the interaction of condensin II with the LINC complex involved in the regulation of centromere positioning, CII-LINC.

CII-LINC and CRWNs independently regulate centromere distribution at different stages of mitosis

As mentioned earlier, no bias in centromere distribution was observed in *crwn1crwn4* mutants by imaging (Fig. 3b, c). However, when the number of distinguishable centromeres in interphase nuclei was counted, the *crwn1crwn4* nuclei had a significantly lower number of centromeres than the wild type, similar to the *cap-h2-2* condensin II mutant (Supplementary Fig. S3), consistent with a previous study using FISH[9,11]. These findings imply that CRWNs contribute to centromere positioning in a manner different from condensin II. To date, CRWNs have been shown to function in tethering chromatin, including pericentromeric and centromeric heterochromatin, to the nuclear periphery[15]. Consistent with this, we found CRWN1 to interact with CENH3 in co-IP assays in tobacco leaves and an enrichment of CRWN1-GFP at tdTomato-CENH3 positive foci in interphase nuclei (Fig. 4a,b). These findings support that CRWNs directly regulate centromere positioning.

To obtain further insights into the function of CRWNs in centromere positioning, we analysed centromere movement in interphase nuclei. Live imaging demonstrated that the centromeres in *crwn1crwn4* mutant

nuclei are highly dynamic, but static in the wild type and mutants affecting CII-LINC, i.e., *cap-h2-2* and *sun1-KOsun2-KD*, which show a biased centromere distribution (Fig. 4c,d). This result indicates that CRWNs restrain the positions of centromeres during interphase at the nuclear periphery. Next, to evaluate the genetic interaction between CII-LINC and CRWNs in the regulation of centromere positioning, we observed centromere dynamics in the triple *cap-h2-2crwn1crwn4* mutant. Intriguingly, we found both types of centromere distribution, biased and scattered, in this triple mutant (Fig. 5a). Subsequently, we monitored centromeres dynamics in the triple mutant (Fig. 5b). First, the triple mutant clearly showed a biased centromere distribution, as observed in *cap-h2-2* (Fig. 2c, from 0 to 5 min in Fig. 5b). Over time, however, the centromeres started moving around and, consequently, adopted a distribution similar to that observed in the wild type (from 10 to 45 min in Fig. 5b), contrasting the biased distribution in *cap-h2-2* (Fig. 2c and Fig. 4c). Even after centromere scattering, centromere movement in the triple mutant was more dynamic than that in wild type or *cap-h2-2* nuclei (Fig 4c,d). These observations suggest that the NE-stabilisation of centromeres by CRWNs occurs continuously during the interphase, and that CII-LINC and CRWNs function independently of each other to regulate centromere positioning.

Considering this, we propose that centromere distribution is determined by a two-step process after the centromere pairs segregate at early anaphase: (i) interactions of CII-LINC with centromeres occur at late anaphase, mediating the scattering of centromeres from late anaphase to telophase, and (ii) CRWNs stabilise the position of scattered centromeres after the entry into interphase (Fig. 5c).

Condensin II and CRWNs make both similar and distinct contributions to chromatin organization

Considering that both CII-LINC and CRWNs have a major impact on centromere distribution, we investigated whether deficiencies in these factors alter higher-order chromatin organization. We performed duplicate Hi-C analysis in Col-0, *cap-h2-2*, *crwn1crwn4*, and *cap-h2-2crwn1crwn4* plants (Supplementary Table 1). A high correlation between the duplicates was obtained (Supplementary Fig. S4a,b), and the combined data from duplicate experiments were used for subsequent analyses to improve resolution. To compare contact frequencies, we calculated the relative differences between all elements of the two Hi-C matrices of interest, as described previously[24] (Fig. 6a). By visual inspection, we found that *cap-h2-2* exhibited increased inter-chromosomal pericentromere contacts and increased contacts between the two centromere-flanking halves of the pericentromeres. Additionally, we observed elevated *cis*-chromosomal inter-arm and *trans*-chromosomal inter-arm contacts. The *cap-h2-2* mutant also showed a conspicuous decrease in pericentromere-arm contacts (both *cis*- and *trans*-chromosomal), and a slight decrease in intra-arm contacts and interactions within centromeres (Supplementary Fig. S5). Similar alterations in chromatin contacts were observed in the *crwn1crwn4* double and *cap-h2-2crwn1crwn4* triple mutants; however, their overall magnitude was greater than that observed in *caph2-2*. These results suggest that the defects in both condensin II and CRWN mutants affect chromatin organization in a similar way. Additionally, a comparison of *crwn1crwn4* and *cap-h2-2crwn1crwn4* showed only slightly more enhanced differences in some interacting regions, including inter-chromosomal pericentromere interactions, *cis*-chromosomal pericentromere-arm interactions, and interactions within each centromere, which are most likely caused by the additional mutation in *CAP-H2*.

These findings suggest that condensin II and CRWNs independently contribute to the organization of chromatin interactions, at least in specific regions.

Next, we analysed the formation of discrete structural domains by calculating the correlation coefficients of the distance-normalised interaction matrix[24] (Fig. 6b). The correlation matrix derived from a Hi-C map is closely related to how strong interactions/depletions are among chromatin regions and, thus, helps to highlight the structural separation between different chromosomal regions. Therefore, a weakened correlation matrix indicates a lower degree of spatial separation of different chromatin compartments[15]. The *cap-h2-2* Hi-C map showed a subtly weaker correlation matrix than the wild type, indicating a slightly less well-defined chromatin compartmentalisation. A more strongly weakened chromatin compartmentalisation was observed in the *crwn1crwn4* Hi-C map, as previously reported for the individual mutants, *crwn1* and *crwn4*[15]. In addition, the *cap-h2-2crwn1crwn4* Hi-C map showed the weakest compartmentalisation.

Next, we performed a principal component analysis on the correlation matrix of each chromosome, including centromeric regions (Fig. 6c). In this analysis, regions exhibiting negative eigenvalues corresponded to B compartments, which, in *Arabidopsis*, mainly cover the constitutive heterochromatin of pericentromeres. We found that the eigenvalue distributions along each of the chromosome arms were similar among the plants analysed. However, both *crwn1crwn4* and *cap-h2-2crwn1crwn4* exhibited a similarly altered eigenvalue distribution pattern around the pericentromeric regions of all chromosomes, with negative eigenvalues expanding into more distal regions of the pericentromeres. Consequently, the eigenvalue boundaries between pericentromeres and chromosome arms became blurred (Fig. 6c). To further evaluate chromatin structure, we determined the interaction decay exponents (IDEs) of entire chromosomes, pericentromeres, and chromosome arms (Fig. 6d). The IDE is indicative of the chromatin structure model, i.e., whether a region behaves according to the fractal- or the equilibrium-globule model[25]. Therefore, no differences in the IDEs of the entire chromosomes and chromosome arms were observed between the mutants and the wild type. However, significantly higher pericentromeric IDEs were observed in *crwn1crwn4* and *cap-h2-2crwn1crwn4* mutants, with IDEs close to those of chromosome arms (Fig. 6d). This suggests a euchromatinisation of parts of the pericentromeres in these mutants. It is worth noting that the eigenvalue distribution and the IDEs of pericentromeres were comparable between *cap-h2-2* and the wild type (Fig. 6c,d). Collectively, these results suggest that CRWNs are involved in the organization of chromatin structure, especially at pericentromeres, establishing a defined compartmentalisation of heterochromatin. In contrast, the contribution of condensin II to chromatin structure was not evident, despite its involvement in chromatin interactions at pericentromeres.

Previous studies reported that the transcriptome is not significantly affected in a *crwn1*-single mutant, which shows weakened chromatin compartmentalisation and higher IDEs at pericentromeres[15,24], similar to the *crwn1crwn4* double mutant used in this study. Our transcriptome analysis of the *crwn1crwn4* double mutant revealed only 83 differentially expressed genes (DEGs). Additionally, the extent of the difference was less than 2-fold in 60% of the DEGs (Supplementary Fig. S6). Similarly, the *cap-2h-2*

mutation had little effect on the transcriptome: there were only 164 DEGs, 129 of which showed less than a 2-fold difference (Supplementary Fig. S6). These results suggest that, in addition to alterations in chromatin organization, abnormal centromere distribution does not strongly influence local gene regulation in mutants affecting CRWNs or condensin II.

Centromere distribution is involved in the maintenance of genome integrity

After evaluating the biological significance of CII-LINC- and CRWN-mediated centromere distribution, we focused on investigating its potential role in maintaining genome integrity. Condensin II ameliorates DNA damage caused by abiotic stress and genotoxic chemical treatments[16]. CRWNs, including CRWN1 and CRWN4, are involved in protecting genomic DNA against oxidative stress caused by methyl methanesulfonate[26,27]. Accordingly, we evaluated the levels of DNA double-strand breaks (DSBs) in the root tips of mutants showing an abnormal centromere distribution under normal conditions using comet assays (Fig. 7a). We confirmed that *cap-h2-2*, *crwn1crwn4*, and *sun1sun2* (a double knockout mutant whose background is Col-0/Ws heterozygote) mutants had increased DSBs compared to the wild type. Additionally, primary root growth was severely delayed in the mutants after 2 and 4 days of treatment with the DSB-inducing reagent zeocin (Fig. 7b). Moreover, *sun1sun2* exhibited a highly deformed root tip, and all mutants showed a reduction in meristem size after 2 days of zeocin treatment (Fig. 7c,d). These results confirm that genome integrity is impaired in mutants with abnormal centromere distribution. Additionally, we found that the *cap-h2-2crwn1crwn4* mutant displayed an additive phenotype compared to *cap-h2-2* and *crwn1crwn4* with respect to DSBs and hypersensitivity to zeocin in terms of primary root growth and root morphology (Fig. 7a,b,c), suggesting that condensin II and CRWNs contribute to the maintenance of genome integrity via different mechanisms.

To assess whether the hypersensitivity of the mutants to DNA damage could be attributed to impaired gene regulation in response to the induction of DNA damage, we performed transcriptome analysis at 0, 1, and 3 h after zeocin treatment (Supplementary Fig. S7). We confirmed that 1h and 3h treatments with zeocin markedly altered the transcriptome in the wild type (Supplementary Fig. S7a). Under these conditions, we compared the transcriptomes of the wild type, *cap-h2-2*, and *crwn1crwn4* and found that all three transcriptomes were similar (Supplementary Fig. S7b). These results suggest that the regulation of gene expression upon DNA damage is normal in both the *cap-h2-2* and *crwn1crwn4* mutants.

Discussion

Compared to the interphase centromere distribution in plants adopting a Rabl configuration, *Arabidopsis* centromeres were considered to be distributed randomly[28]. However, previous studies using a spatial statistics approach found a more regular distribution of centromeres than expected under the assumption of randomness. Interactions of the centromeres with certain nuclear factors, including the NE, was proposed to contribute to this specific distribution[29,30]. Here, we reveal a novel mechanism for centromere distribution in interphase nuclei that can be divided into two steps: (i) a scattering step dependent on interactions of the centromere with the CII-LINC complex during mitosis, and (ii) a stabilising step

dependent on interaction of the centromere with the nuclear lamina throughout interphase (Fig. 5c). This two-step process substantially contributes to the spatial regularity of centromeres in *Arabidopsis*.

We propose that condensin II mediates the association of centromeres with the NE during mitosis by interacting with the LINC complex, playing an essential role in centromere scattering in *Arabidopsis* (Fig. 5c). A different model was proposed for human cells, where the lengthwise compaction of chromosomes by condensin II during mitosis determines the interphase centromere distribution[31]. In contrast, a role for interphase condensin II in regulating centromere distribution has been reported in *Drosophila melanogaster.* Enhanced interphase condensin II activity drives the force that separates and scatters clustered centromeres around the nuclear periphery by promoting the axial compaction of chromosomes in the polyploid nuclei of nurse cells[32]. Either way, condensin II plays a determining role in regulating centromere distribution in eukaryotes including *Arabidopsis* (Fig. 3c)[9,10,31,32].

Unlike in the condensin II mutant, the centromere localisation bias in mutants of nuclear envelop proteins was low (Fig. 3b-e). This suggests functional redundancy between SUN and KASH proteins. There may also be other unidentified proteins involved in condensin II-mediated centromere scattering. A similar idea was proposed for nuclear lamina-mediated centromere stabilisation. At least, the known CRWN-interacting proteins, KAKU4[33], SUN1, and SUN2[34], are unlikely to be involved in this process (Fig. 4b,c)[15]. Moreover, absence of CRWN1 and CRWN2 does not result in the dissociation of centromeres from the NE during interphase[13], suggesting the existence of other proteins required for NE association of centromeres in interphase (Fig. 5c). Intriguingly, NUCLEOPORIN1, a component of the nuclear pore complex (NPC), directly interacts with pericentromeric chromatin[15,35] and CRWNs[36], indicating its possible function in interphase centromere distribution. A recent study comprehensively identified putative NE integral proteins, the nuclear factors associated with the NE[37]. Future characterisation of known NPC components and novel NE-related proteins with respect to centromere association with the NE will be needed to fully understand how the position of centromeres is regulated during the cell cycle in *Arabidopsis*.

Previous studies in yeast[38,39], *D. melanogaster*[40,41], and human cells[42] have proposed a role for centromere clustering in determining the spatial organization of chromosomes during interphase. However, the significance of adopting a scattered centromere distribution in nuclear events remains unknown. In this study, Hi-C analysis revealed that the defects in both types of centromere positioning, scattering and stabilisation, clearly altered genome-wide chromatin organization, including inter-chromosomal interactions (Fig. 6a,b). However, these alterations were not accompanied by widespread changes in gene expression (Supplementary Fig. S6), which is in agreement with the moderate effects on the transcriptome in another condensin II mutant, *cap-d3*[43]*.* Moreover, *crwn1* single and *crwn1crwn4* double mutants showed similar effects on chromatin interactions[15,24]. These results indicate a robustness of local chromatin organization associated with gene regulation, despite marked changes in centromere distribution.

In contrast, DNA damage hypersensitivity was found to be a common phenotype among mutants defective in centromere distribution (Fig. 7). There are two main explanations for this hypersensitivity: (i) impaired repair of damaged DNA or (ii) impaired maintenance of genome stability which is required to avoid damage. Since the gene expression response to DNA damage was not majorly affected in the mutants (Supplementary Fig. S7), the latter is more likely. In *Saccharomyces cerevisiae* and *D. melanogaster*, both having chromosomes in Rabl configuration, the destabilisation of centromere positioning causes genome instability, which may be caused by the impaired silencing of transposable elements and repetitive DNA[44–46]. However, enhanced expression of transposable elements was not observed in either the *cap-h2-2* or *crwn1crwn4* mutant (Supplementary Data), suggesting that there is another cause of genome instability in plants. Additionally, our Hi-C analysis suggested the importance of centromere stabilisation in the structural organization of pericentromeric regions (Fig. 6c,d). The centromere is considered to be intrinsically fragile, most likely due to the high density of repetitive sequences, resulting in its susceptibility to DNA stress[47]. Therefore, it is tempting to speculate that the aberrant organization of pericentromeric chromatin makes centromeres more vulnerable. In conclusion, centromere distribution seems to be linked to genome stability but not to gene regulation in *Arabidopsis*.

Methods

Plant materials and growth conditions

If not mentioned otherwise, all plants used were *Arabidopsis thaliana* (L.) Heynh. of the Columbia (Col-0) accession. The *cap-h2-2*[16], *cap-g2-1*[16], *wifi*[48], *sun1-KOsun2-KD*[20], *sun1sun2* double KO (the background is Clol-0/Ws heterozygote)[49], *sun4sun5*[50], *myosin xi-i* (*kaku1-4;* SALK_082443)[51], *sine1-1*[52], and *crwn1crwn4*[53] mutants have been described previously. The *cap-h2crwn1crwn4* mutant was generated by crossing *cap-h2-2* and *crwn1crwn4.* The primers used to confirm T-DNA insertions are listed in Supplementary Table 2. In all experiments, seeds were sown on media containing MGRL solution, 1% (w/v) sucrose, and 1.5% (w/v) gellan gum[16]. After a 1-day incubation at 4 °C, the plates were placed vertically in a growth chamber (16-h light/8-h dark cycle, 22 °C) until analysis.

DNA damage treatment and subsequent analyses

For the DNA damage sensitivity test, 5-day-old seedlings pre-incubated on vertically oriented MGRL plates were transferred to plates containing various concentrations of zeocin (Invitrogen, Carlsbad, CA, USA), and their primary root-tip positions were marked. After 4 days of incubation, the lengths of the newly elongated primary roots from the marked positions were determined using ImageJ software (http://rsb.info.nih.gov/ij/). The same plants were also stained with 10 μg/ml propidium iodide (PI) (Molecular Probes, Eugene, OR, USA) and subsequently subjected to confocal imaging analysis.

For microarray analysis, 14-day-old seedlings pre-incubated on vertically oriented MGRL plates were transferred to a container containing half-strength MGRL solution without sucrose. After 3 h of acclimation to hydroponic conditions, the seedlings were transferred to different containers containing

half-strength MGRL solution with 10 μM zeocin. Whole roots were harvested after treatment with zeocin for 0, 1, and 3 h, and subsequently subjected to total RNA extraction and microarray analysis.

Microarray analysis

Total RNA was extracted from whole roots of seedlings using PureLink® Plant RNA Reagent (Thermo Fisher Scientific) following the manufacturer's protocol. Microarray analysis was performed using an Agilent Arabidopsis microarray platform, as previously described[54]. RMA normalisation was performed for signals of microarray probes using the limma package[55] in R (version 2.12.1) (R Core Team). The statistical significance of differences in gene expression was determined using Student's *t-test* and a Benjamini Hochberg corrected false discovery rate (FDR)[56]. The microarray data are available on the GEO website (GEO ID: GSE179466 for Supplemental Data 1; GSE179793 for Supplemental Data 2).

Comet assay

Nuclei were collected from 1 cm root tips of 5-day-old seedlings incubated on vertically oriented MGRL plates. A CometAssay® Reagent Kit for Single Cell Gel Electrophoresis Assay (Trevigen, Gaithersburg, MD, USA) was used to perform comet assays, as described previously[57]. Images were analysed using the ImageJ software plugin CometAssay distributed by the University of North Carolina School of Medicine, USA (https://www.med.unc.edu/microscopy/resources/imagej-plugins-and-macros/comet-assay).

Generation of transgenic plants

Plants expressing *pCAP-G2::CAP-G2-GFP*[16], *pCAP-G2::CAP-G2-GFP*[16], and *p35S::CRWN1-GFP*[53] have previously been established. Using an amplified clone of the genomic *CAP-D3* fragment, a vector pMDC107[58] containing *pCAP-D3::CAP-D3-GFP* was constructed as described previously[16]. To visualise centromeres and nuclei, plants were transformed with *Agrobacterium tumefaciens* (strain GV3101 pMP90) harbouring the vector pMDC99[58] containing *p35S::tdTomato-CENH3*[59] and a vector pMDC100[58] containing *pRPS5a::H2B-GFP*[60]. The final plasmid was mobilised into *Agrobacterium tumefaciens* (strain GV3101 pMP90) and used for transformation of plants together with another *Agrobacterium tumefaciens* strain harbouring the vector pMDC99 containing *p35S::VENUS-CENH3*. Transgenic plants were selected on medium containing 1/2× Murashige and Skoog salts, 1% sucrose, 20 μg/ml hygromycin B, and 250 μg/ml claforan. The fluorescence of tdTomato and GFP was confirmed in the T1 plants. T2 plants were used for the analysis. The primers used for cloning the *CAP-D3* genomic fragment is listed in Supplemental Table 2.

Confocal imaging

One-week-old plants were used for confocal imaging, unless stated otherwise. For time-lapse imaging of CAP-G2-GFP and the imaging of PI-stained roots, the roots were observed under an FV1200 inverted laser confocal microscope equipped with a GaAsP detector (Olympus, Tokyo, Japan) using a 473 nm LD laser for GFP and 559 nm LD laser for PI. To image CAP-G2-GFP, CAP-H2-GFP, CAP-D3-GFP, CENH3-tdTomato,

CENH3-Venus, and H2B-GFP, the roots of the samples were observed under an inverted fluorescence microscope (IX81; Olympus), which included a laser (488 nm for GFP and 561 nm for tdTomato detection) equipped with a confocal scanning unit (CSU-X1; Yokogawa, Tokyo, Japan) and an Andor Neo 5.5 sCMOS camera (Oxford Instruments, Oxfordshire, UK). The *z*-stacks were reconstructed into a maximum projection view using ImageJ software. The trajectories of centromeres were analysed using the ImageJ software plugin MTrackJ (https://imagescience.org/meijering/software/mtrackj/).

Co-immunoprecipitation assay

The coding sequences without the stop codon of *CAP-G2*, *CENH3, SUN1*, and *SUN2* were amplified from *Arabidopsis* cDNA. The clones of *CAP-G2* and *CENH3* were subcloned into the pENTR-D/TOPO vector, and *SUN1* and *SUN2* were subcloned into the pDonr201 vector, according to the manufacturer's protocol. The primers used for cloning are listed in Supplementary Table 2. By LR recombination with LR clonase II, the fragment of CAP-G2 was transferred to pMDC43 and the fragments of *SUN1*, *SUN2*, and *CENH3* were transferred to pGWB541 or pGWB560 to construct Gateway destination vectors harbouring the GFP- or tagRFP-fused target protein driven by the CaMV *35S* promoter. The final plasmids were mobilised into *Agrobacterium tumefaciens* (strain GV3101 pMP90).

The fluorescent fusion proteins were transiently expressed in *Nicotiana benthamiana* leaves by *Agrobacterium*-mediated infiltration, as previously described[11]. The leaves were harvested 4 or 5 days after inoculation. Immunoprecipitation was performed using a μMACS GFP Isolation Kit (Miltenyi Biotec, Auburn, CA, USA). The leaves (1.0–2.0 g) were homogenised in two volumes of μMACS lysis buffer containing a protease inhibitor cocktail for plant cell and tissue extracts (Sigma-Aldrich, St. Louis, MO, USA). The lysate was then filtered through two layers of Miracloth (Merck, Hamburg, Germany), mixed with anti-GFP antibody-conjugated magnetic beads, and incubated at 4 °C for 30 min. The GFP-fusion proteins were purified using a magnetic column according to the manufacturer's protocol. Anti-GFP antibody (ab290; Abcam, Cambridge, UK) (1:1000) and anti-tagRFP antibody (R10367; Thermo Fisher Scientific, Waltham, MA, USA) (1:500) were used as primary antibodies. A horseradish peroxidase (HRP)-conjugated anti-rabbit antibody pAb-HRP (458, MBL, Tokyo, Japan) (1:10000) was used as the secondary antibody. Chemiluminescence from the target proteins of each antibody was visualised using ImmunoStar LD (Wako, Osaka, Japan) on a Fusion Pulse system (Vilber Lourmat, Marne-la-Vallée, France).

Yeast two-hybrid assay

The vectors, pENTR-D/TOPO harbouring *CAP-H2* or *GAP-G2* and pDonr201 harbouring *SUN1* or *SUN2* were prepared as described above. By LR recombination with LR clonase II (Invitrogen), the fragments were transferred to pDEST_GADT7 or pDEST_GBKT7. The Y2HGold yeast strain (Takara Bio, Shiga, Japan) was transformed using the Frozen-EZ Yeast Transformation II kit (Zymo Research, Irvine, CA, USA). Transformants were selected on SD/-Leu/-Trp medium. Protein interactions were analysed on SD/-Leu/-Trp/-His/-Ade medium. pGADT7 and pGBKT7 were used as negative controls.

Bi-FC assay

The coding sequences without the stop codon of *CAP-G2* and *CAP-H2* were amplified from *Arabidopsis* cDNA, while *uidA* encoding b-glucuronidase (GUS) was amplified from pMDC162, followed by subcloning into the pENTR-D/TOPO vector. The vectors pDonr201 harbouring *SUN1* or *SUN2* were prepared as described above. By LR recombination with LR clonase II, the fragments were transferred to pGWB vectors containing the N-terminal YFP (pnYGW) or C-terminus YFP (pcYGW) for the Bi-FC assays[61]. To visualise the nuclei, a vector pMDC100 containing *35S::H2B-tdTomato* was used.

Constructs were transiently expressed in tobacco BY-2 cells, as previously described[62]. Four ml of cell suspension of 3-day-old BY-2 cells were pipetted onto filter paper, and the cells were bombarded with gold particles (1.0 μM) coated with the appropriate vector constructs using a particle delivery system (PDS-1000/He; BioRad, Hercules, CA, USA) according to the manufacturer's recommendations. The particles were bombarded into the cells in a vacuum gauge of 28 in Hg at a helium pressure of 1,100 p.s.i. Then, the cells were 2-fold diluted with medium for cell culture and kept in the dark at 27 °C for 16–20 h to go through at least one cell cycle before observing them under an inverted laser confocal microscope (FV1200).

Hi-C sample preparation

Aerial parts (~2.0 g) of two-week-old seedlings were used for Hi-C sample preparation. Nuclei isolation, digestion with HindIII, fill-in biotinylation, ligation, and purification of the Hi-C samples were performed as previously described[63]. For the preparation of the sequencing library, the purified Hi-C sample (500 ng) was diluted to 500 μl with dH_2O, and 500 μl of 2× binding buffer (BB) (10 mM Tris, 1 mM EDTA, 2 M NaCl) was added. The diluted Hi-C samples were fragmented to a mean size of 300 bp by sonication using a Covaris M220 sonication system (Covaris, Woburn, MA, USA) in a milliTUBE 1 ml AFA Fibre (Covaris). The parameters of the program were as follows: power mode, frequency sweeping; time, 20 min; duty cycle, 5%; intensity, 4; cycles per burst, 200; temperature (water bath), 6 °C. Biotin-labelled Hi-C samples were then enriched using MyOne Streptavidin C1 magnetic beads (Veritas, Tokyo, Japan). For this, 60 μl of streptavidin beads were washed twice with 400 μl of Tween Wash Buffer (TWB) (5 mM Tris, 0.5 mM EDTA, 1M NaCl, 0.05% Tween-20). The recovery of streptavidin beads was performed by placing the tubes on a magnetic stand. Subsequently, the beads were added to 1 ml of sheared Hi-C sample. After 15 min of incubation at room temperature under rotation, the supernatant was removed, and the beads binding biotinylated Hi-C fragments were resuspended in 400 μl of 1× BB. Then, the beads were washed once in 60 μl RSB (Resuspension buffer) (Illumina, San Diego, CA, USA), and finally resuspended in 50 μl RSB. The enriched biotinylated DNA fragments were subjected to library construction on beads using the KAPA HyperPrep Kit for Illumina (Roche, Basel, Switzerland) according to the manufacturer's protocol, with 18 cycles of PCR for library amplification. The amplified DNA fraction (50 μl) was corrected and purified using Agencourt AMPure XP (Beckman Coulter) following the standard protocol, and finally resuspended in 15 μl of RSB. The Hi-C libraries were sequenced on a NextSeq 500 sequencer (Illumina) in the 150 bp paired-end mode (Supplementary Table 1).

Hi-C data analysis

Raw Hi-C sequencing reads were trimmed to 30 bp and aligned using subread-align[64] with the parameters: -u (unique only), -I 0 (no indels), -M 0 (no mismatches). Subsequently, the aligned Hi-C data was further processed with the help of HiCdat[65] and contact matrices of 50 kb and 100 kb bin sizes were generated (see Supplementary Table S1 for number of valid contacts). The minimal distance to filter inward pairs was set to 1 kb and to filter outwards-facing pairs to 25 kb. Pairs fulfilling these criteria have not been included in the Hi-C matrices. Distance-normalization has been performed while loading the data using f.load.samples() function including 25 repetitions in an R-package HiCdatR[65]. Distance decay (IDEs) calculation, differential analysis, correlation analysis between samples, and analysis of first principal component (PCA) were also performed using HiCdatR. PCA analyses were performed on entire chromosome lengths. All analyses were performed using 50 kb or 100 kb genomic bin size. Genomic coordinates of pericentromeric regions to calculate IDEs were defined as follows: Chr1: 10Mb-18Mb, Chr2: 1Mb-8Mb, Chr3: 10Mb-17Mb, Chr4: 1.5Mb-6.5Mb, Chr5: 9Mb-16Mb.

Declarations

Acknowledgments

We thank Ms. Sayoko Mibu, Ms. Yuka Asako (Tokyo Univ. Sci., Japan), and Dr. Yayoi Inui (Univ. Tokyo, Japan) for substantial technical assistance. This research was supported by grants from Takeda Science Foundation and Tokyo University of Science Grant for International Joint Research to T.S., grants from MXT/JSPS KAKENHI (15H05955, 15H05962, 19H03259, and 20H03297) and JST CREST (grant number JPMJCR20S6) to S.M., as well as the University of Zurich and a grant from the European Research Council (ERC AdG Nr. 243996) to U.G.

Contributions

T.Sa., Y.S., and S.M. designed the experiments. T.Sa., Y.S., S.G., and S.M. wrote the manuscript. T.Sa., Y.S., T.Y., N.I., Y.O., T.Sug., and T.H. performed the experiments and analyzed the data. T.Suz. performed sequencing. S.G. analyzed Hi-C data. M.T. performed microarray experiments and A.M. analyzed microarray data. S.H., M.S., U.G., and S.M. supervised the project. T.Sa., U.G., and S.M. raised funding, All authors contributed through discussions and reviewed the manuscript.

References

1. Matsunaga, S. *et al.* New Insights into the Dynamics of Plant Cell Nuclei and Chromosomes. in *International Review of Cell and Molecular Biology* (ed. Jeon, K. W.) vol. 305 253–301 (Academic Press, 2013).
2. Muller, H., Gil, J. & Drinnenberg, I. A. The Impact of Centromeres on Spatial Genome Architecture. *Trends Genet.* **35**, 565–578 (2019).

3. Schubert, I. & Shaw, P. Organization and dynamics of plant interphase chromosomes. *Trends Plant Sci.* **16**, 273–281 (2011).
4. Vanrobays, E., Thomas, M. & Tatout, C. Heterochromatin Positioning and Nuclear Architecture. in *Annual Plant Reviews online* 157–190 (American Cancer Society, 2017). doi:10.1002/9781119312994.apr0502.
5. Dong, F. & Jiang, J. Non-Rabl Patterns of Centromere and Telomere Distribution in the Interphase Nuclei of Plant Cells. *Chromosome Res.* **6**, 551–558 (1998).
6. Oko, Y., Ito, N. & Sakamoto, T. The mechanisms and significance of the positional control of centromeres and telomeres in plants. *J. Plant Res.* **133**, 471–478 (2020).
7. Fang, Y. & Spector, D. L. Centromere Positioning and Dynamics in Living *Arabidopsis* Plants. *Mol. Biol. Cell* **16**, 5710–5718 (2005).
8. Roberts, N. Y., Osman, K. & Armstrong, S. J. Telomere Distribution and Dynamics in Somatic and Meiotic Nuclei of *Arabidopsis thaliana*. *Cytogenet. Genome Res.* **124**, 193–201 (2009).
9. Sakamoto, T., Sugiyama, T., Yamashita, T. & Matsunaga, S. Plant condensin II is required for the correct spatial relationship between centromeres and rDNA arrays. *Nucleus* **10**, 116–125 (2019).
10. Schubert, V., Lermontova, I. & Schubert, I. The *Arabidopsis* CAP-D proteins are required for correct chromatin organization, growth and fertility. *Chromosoma* **122**, 517–533 (2013).
11. Sakamoto, Y. *et al.* Subnuclear gene positioning through lamina association affects copper tolerance. *Nat. Commun.* **11**, 5914 (2020).
12. Dittmer, T. A., Stacey, N. J., Sugimoto-Shirasu, K. & Richards, E. J. *LITTLE NUCLEI* Genes Affecting Nuclear Morphology in *Arabidopsis thaliana*. *Plant Cell* **19**, 2793–2803 (2007).
13. Poulet, A. *et al.* The LINC complex contributes to heterochromatin organization and transcriptional gene silencing in plants. *J. Cell Sci.* **130**, 590–601 (2017).
14. Wang, H., Dittmer, T. A. & Richards, E. J. Arabidopsis CROWDED NUCLEI (CRWN) proteins are required for nuclear size control and heterochromatin organization. *BMC Plant Biol.* **13**, 200 (2013).
15. Hu, B. *et al.* Plant lamin-like proteins mediate chromatin tethering at the nuclear periphery. *Genome Biol.* **20**, 87 (2019).
16. Sakamoto, T. *et al.* Condensin II Alleviates DNA Damage and Is Essential for Tolerance of Boron Overload Stress in *Arabidopsis*. *Plant Cell* **23**, 3533–3546 (2011).
17. Fujimoto, S. *et al.* Characterization and dynamic analysis of *Arabidopsis* condensin subunits, AtCAP-H and AtCAP-H2. *Planta* **222**, 293–300 (2005).
18. Collette, K. S., Petty, E. L., Golenberg, N., Bembenek, J. N. & Csankovszki, G. Different roles for Aurora B in condensin targeting during mitosis and meiosis. *J. Cell Sci.* **124**, 3684–3694 (2011).
19. Fujiwara, T., Tanaka, K., Kuroiwa, T. & Hirano, T. Spatiotemporal dynamics of condensins I and II: evolutionary insights from the primitive red alga *Cyanidioschyzon merolae*. *Mol. Biol. Cell* **24**, 2515–2527 (2013).

20. Oda, Y. & Fukuda, H. Dynamics of *Arabidopsis* SUN proteins during mitosis and their involvement in nuclear shaping. *Plant J.* **66**, 629–641 (2011).
21. Masuda, K., Haruyama, S. & Fujino, K. Assembly and disassembly of the peripheral architecture of the plant cell nucleus during mitosis. *Planta* **210**, 165–167 (1999).
22. Meier, I., Richards, E. J. & Evans, D. E. Cell Biology of the Plant Nucleus. *Annu. Rev. Plant Biol.* **68**, 139–172 (2017).
23. Sakamoto, Y. Nuclear lamina CRWN proteins regulate chromatin organization, gene expression, and nuclear body formation in plants. *J. Plant Res.* **133**, 457–462 (2020).
24. Grob, S., Schmid, M. W. & Grossniklaus, U. Hi-C Analysis in *Arabidopsis* Identifies the *KNOT*, a Structure with Similarities to the *flamenco* Locus of *Drosophila*. *Mol. Cell* **55**, 678–693 (2014).
25. Lieberman-Aiden, E. *et al.* Comprehensive Mapping of Long-Range Interactions Reveals Folding Principles of the Human Genome. *Science* **326**, 289–293 (2009).
26. Hirakawa, T. & Matsunaga, S. Characterization of DNA Repair Foci in Root Cells of *Arabidopsis* in Response to DNA Damage. *Front. Plant Sci.* **10**, (2019).
27. Wang, Q. *et al.* Roles of CRWN-family proteins in protecting genomic DNA against oxidative damage. *J. Plant Physiol.* **233**, 20–30 (2019).
28. Pecinka, A. *et al.* Chromosome territory arrangement and homologous pairing in nuclei of *Arabidopsis thaliana* are predominantly random except for NOR-bearing chromosomes. *Chromosoma* **113**, 258–269 (2004).
29. Andrey, P. *et al.* Statistical Analysis of 3D Images Detects Regular Spatial Distributions of Centromeres and Chromocenters in Animal and Plant Nuclei. *PLOS Comput. Biol.* **6**, e1000853 (2010).
30. Arpòn, J., Sakai, K., Gaudin, V. & Andrey, P. Spatial modeling of biological patterns shows multiscale organization of *Arabidopsis thaliana* heterochromatin. *Sci. Rep.* **11**, 323 (2021).
31. Hoencamp, C. *et al.* 3D genomics across the tree of life reveals condensin II as a determinant of architecture type. *Science* **372**, 984–989 (2021).
32. Bauer, C. R., Hartl, T. A. & Bosco, G. Condensin II Promotes the Formation of Chromosome Territories by Inducing Axial Compaction of Polyploid Interphase Chromosomes. *PLOS Genet.* **8**, e1002873 (2012).
33. Goto, C., Tamura, K., Fukao, Y., Shimada, T. & Hara-Nishimura, I. The Novel Nuclear Envelope Protein KAKU4 Modulates Nuclear Morphology in *Arabidopsis*. *Plant Cell* **26**, 2143–2155 (2014).
34. Graumann, K. Evidence for LINC1-SUN Associations at the Plant Nuclear Periphery. *PLOS ONE* **9**, e93406 (2014).
35. Bi, X. *et al.* Nonrandom domain organization of the *Arabidopsis* genome at the nuclear periphery. *Genome Res.* **27**, 1162–1173 (2017).
36. Mermet, S. *et al.* Evolutionary conserved protein motifs drive attachment of the plant nucleoskeleton at nuclear pores. *bioRxiv* 2021.03.20.435662 (2021) doi:10.1101/2021.03.20.435662.

37. Tang, Y., Huang, A. & Gu, Y. Global profiling of plant nuclear membrane proteome in *Arabidopsis*. *Nat. Plants* **6**, 838–847 (2020).
38. Jin, Q. W., Fuchs, J. & Loidl, J. Centromere clustering is a major determinant of yeast interphase nuclear organization. *J. Cell Sci.* **113**, 1903–1912 (2000).
39. Tjong, H., Gong, K., Chen, L. & Alber, F. Physical tethering and volume exclusion determine higher-order genome organization in budding yeast. *Genome Res.* **22**, 1295–1305 (2012).
40. Hou, C., Li, L., Qin, Z. S. & Corces, V. G. Gene Density, Transcription, and Insulators Contribute to the Partition of the *Drosophila* Genome into Physical Domains. *Mol. Cell* **48**, 471–484 (2012).
41. Sexton, T. *et al.* Three-Dimensional Folding and Functional Organization Principles of the *Drosophila* Genome. *Cell* **148**, 458–472 (2012).
42. Tjong, H. *et al.* Population-based 3D genome structure analysis reveals driving forces in spatial genome organization. *Proc. Natl. Acad. Sci.* **113**, E1663–E1672 (2016).
43. Municio, C. *et al.* The *Arabidopsis* condensin CAP-D subunits arrange interphase chromatin. *New Phytol.* **230**, 972–987 (2021).
44. Mekhail, K., Seebacher, J., Gygi, S. P. & Moazed, D. Role for perinuclear chromosome tethering in maintenance of genome stability. *Nature* **456**, 667–670 (2008).
45. Peng, J. C. & Karpen, G. H. H3K9 methylation and RNA interference regulate nucleolar organization and repeated DNA stability. *Nat. Cell Biol.* **9**, 25–35 (2007).
46. Padeken, J. *et al.* The Nucleoplasmin Homolog NLP Mediates Centromere Clustering and Anchoring to the Nucleolus. *Mol. Cell* **50**, 236–249 (2013).
47. Barra, V. & Fachinetti, D. The dark side of centromeres: types, causes and consequences of structural abnormalities implicating centromeric DNA. *Nat. Commun.* **9**, 4340 (2018).
48. Zhou, X. & Meier, I. Efficient plant male fertility depends on vegetative nuclear movement mediated by two families of plant outer nuclear membrane proteins. *Proc. Natl. Acad. Sci.* **111**, 11900–11905 (2014).
49. Varas, J. *et al.* Absence of SUN1 and SUN2 proteins in *Arabidopsis thaliana* leads to a delay in meiotic progression and defects in synapsis and recombination. *Plant J.* **81**, 329–346 (2015).
50. Graumann, K. *et al.* Characterization of two distinct subfamilies of SUN-domain proteins in *Arabidopsis* and their interactions with the novel KASH-domain protein AtTIK. *J. Exp. Bot.* **65**, 6499–6512 (2014).
51. Tamura, K. *et al.* Myosin XI-i Links the Nuclear Membrane to the Cytoskeleton to Control Nuclear Movement and Shape in *Arabidopsis*. *Curr. Biol.* **23**, 1776–1781 (2013).
52. Zhou, X., Graumann, K., Wirthmueller, L., Jones, J. D. G. & Meier, I. Identification of unique SUN-interacting nuclear envelope proteins with diverse functions in plants. *J. Cell Biol.* **205**, 677–692 (2014).
53. Sakamoto, Y. & Takagi, S. LITTLE NUCLEI 1 and 4 Regulate Nuclear Morphology in *Arabidopsis thaliana*. *Plant Cell Physiol.* **54**, 622–633 (2013).

54. Matsui, A. *et al.* Novel Stress-Inducible Antisense RNAs of Protein-Coding Loci Are Synthesized by RNA-Dependent RNA Polymerase. *Plant Physiol.* **175**, 457–472 (2017).
55. Ritchie, M. E. *et al.* limma powers differential expression analyses for RNA-sequencing and microarray studies. *Nucleic Acids Res.* **43**, e47 (2015).
56. Benjamini, Y. & Hochberg, Y. Controlling the False Discovery Rate: A Practical and Powerful Approach to Multiple Testing. *J. R. Stat. Soc. Ser. B Methodol.* **57**, 289–300 (1995).
57. Sakamoto, T. *et al.* Proteasomal degradation of BRAHMA promotes Boron tolerance in *Arabidopsis*. *Nat. Commun.* **9**, 5285 (2018).
58. Curtis, M. D. & Grossniklaus, U. A Gateway Cloning Vector Set for High-Throughput Functional Analysis of Genes *in Planta*. *Plant Physiol.* **133**, 462–469 (2003).
59. Kurihara, D., Matsunaga, S., Uchiyama, S. & Fukui, K. Live cell imaging reveals plant Aurora kinase has dual roles during mitosis. *Plant Cell Physiol.* **49**, 1256–1261 (2008).
60. Maruyama, D. *et al.* Independent Control by Each Female Gamete Prevents the Attraction of Multiple Pollen Tubes. *Dev. Cell* **25**, 317–323 (2013).
61. Nakagawa, T. *et al.* Improved Gateway Binary Vectors: High-Performance Vectors for Creation of Fusion Constructs in Transgenic Analysis of Plants. *Biosci. Biotechnol. Biochem.* **71**, 2095–2100 (2007).
62. Higaki, T., Kutsuna, N., Okubo, E., Sano, T. & Hasezawa, S. Actin Microfilaments Regulate Vacuolar Structures and Dynamics: Dual Observation of Actin Microfilaments and Vacuolar Membrane in Living Tobacco BY-2 Cells. *Plant Cell Physiol.* **47**, 839–852 (2006).
63. Grob, S. & Grossniklaus, U. Chromatin Conformation Capture-Based Analysis of Nuclear Architecture. in *Plant Epigenetics: Methods and Protocols* (ed. Kovalchuk, I.) 15–32 (Springer US, 2017). doi:10.1007/978-1-4899-7708-3_2.
64. Liao, Y., Smyth, G. K. & Shi, W. The Subread aligner: fast, accurate and scalable read mapping by seed-and-vote. *Nucleic Acids Res.* **41**, e108 (2013).
65. Schmid, M. W., Grob, S. & Grossniklaus, U. HiCdat: a fast and easy-to-use Hi-C data analysis tool. *BMC Bioinformatics* **16**, 277 (2015).

Supplementary Figure Captions

Supplementary Figure S1. Spot-like condensin II localisation in nuclei of the root meristem.

Condensin II localisation visualised by fluorescent protein (green) produced by the *pCAP-H2::CAP-H2-GFP* and *pCAP-D3::CAP-D3-GFP* transgenes in interphase nuclei in the root meristem around the stem cell niche (the root-tip is on the right). Arrowheads indicate nuclei with a spot-like localisation of condensin II. The images are shown as maximum *z*-projections. Bars = 50 µm.

Supplementary Figure S2. Condensin II components interact with SUN proteins.

Bi-FC assays showing that condensin II subunits GAP-G2 and CAP-H2 interact with SUNs *in planta*. Different combinations of genes were transiently expressed in tobacco BY-2 cells as positive and negative controls. Bar = 5 μm.

Supplementary Figure S3. Mutations affecting condensin II and CRWNs reduce the number of separated centromere signals.

The number of separated centromere signals per nucleus was counted. Centromeres were visualised using *35S::tdTomato-CENH3.* The frequency distribution of the number of centromere signals in each mutant was statistically compared to that in the wild type using a *chi*-squared test (*, $p < 0.01$, n = 40).

Supplementary Figure S4. Validation of Hi-C data.

a, Comparison of genome-wide Hi-C maps from various samples (bin size: 50 kb).

b, Enrichment of interaction frequencies, obtained by calculating the relative difference between Hi-C maps of the two respective biological replicates (bin size: 50 kb).

Supplementary Figure S5. Regions of chromatin interactions described in the manuscript.

Magnified images of chromatin interactions in chromosomes 4 and 5 in *cap-h2crwn1/4* are shown in Figure 6a. The regions pointing to each type of chromatin interaction we described are shown.

Supplementary Figure S6. Differentially expressed genes in mutants showing abnormal centromere distribution.

Numbers of up- and down-regulated genes in *cap-h2-2* and *crwn1/4* mutants compared to the wild type are shown (threshold $\geq \sqrt{2}$, FDR < 0.1, $p < 0.05$) (n = 3).

Supplementary Figure S7. Gene expressions in response to DNA damage induction are comparable between the wild type and the defective in centromere positioning.

a, Altered gene expression in wild-type roots (n = 4) after one and three hours of DNA damage treatments.

b, Comparison of gene expression in response to DNA damage treatments between wild-type and mutant plants. The levels of respective gene expression are shown as log2 values (**a**,**b**) (n = 4).

Figures

Fig.1

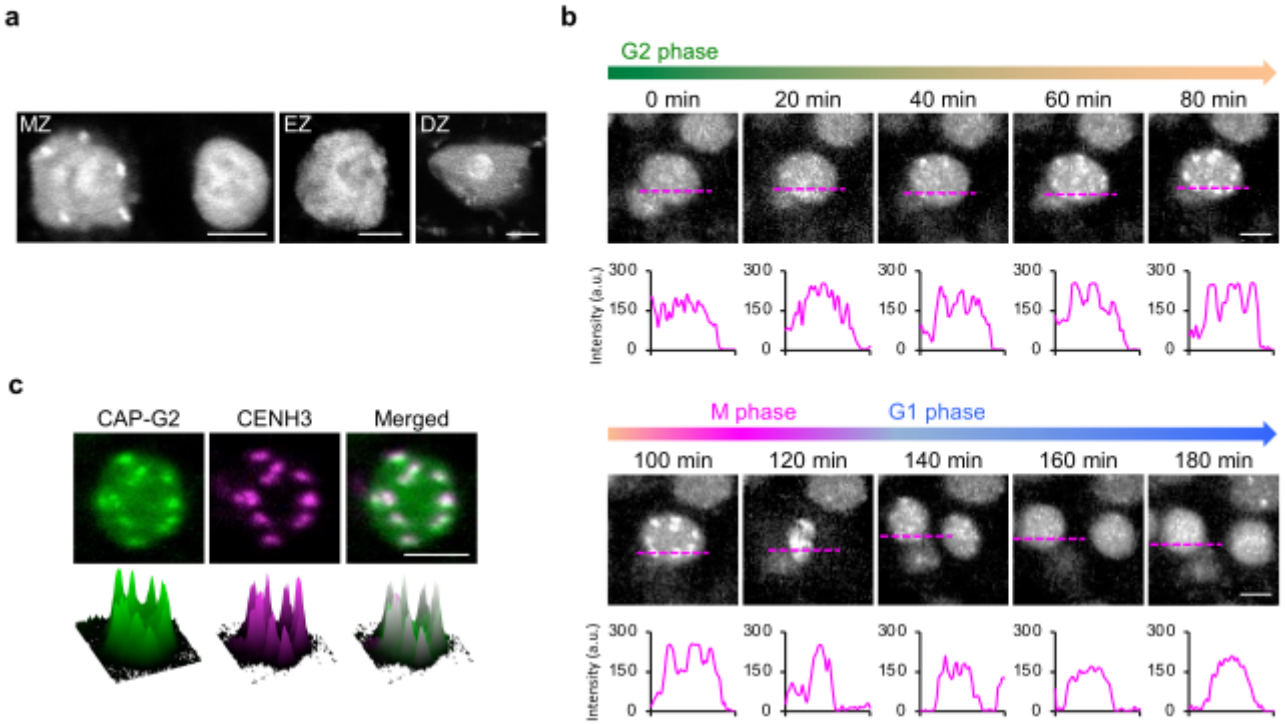

Figure 1

Condensin II is enriched at centromeres from late G2 through early G1 phase a, Condensin II localisation visualised by green fluorescent protein (GFP)_produced from a pCAP-G2::CAP-G2-GFP transgene in interphase nuclei of the root meristematic zone (MZ), elongation zone (EZ), and differentiation zone (DZ). The left and right nuclei in the MZ showed spot-like and scattered localisations, respectively. Bars = 5 μm. b, Condensin II dynamics during mitosis in the root meristem (20 min intervals) as visualised by a pCAP-G2::CAP-G2-GFP transgene. The graphs below show the intensity of CAP-G2-GFP fluorescence measured

by scanning along the dotted magenta lines. The scan length was 12.4 μm. Bars = 5 μm. c, Simultaneous observation of CAP-G2 and CENH3 visualised by pCAP-G2::CAP-G2-GFP and p35S::tdTomato-CENH3 transgenes, respectively, in interphase nuclei of the MZ. The upper images are shown as maximum z-projections. The lower images show three-dimensional images of fluorescence intensity. Bar = 5 μm.

Fig.2

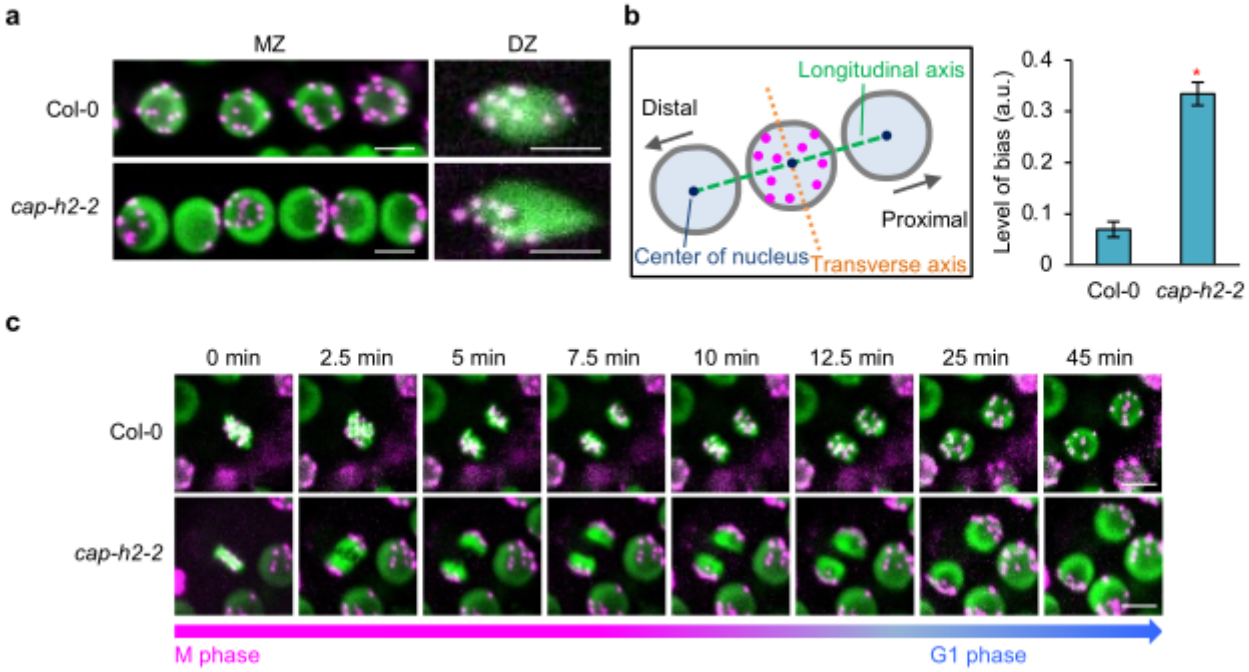

Figure 2

Condensin II is required to form the scattered distribution of centromeres a, Distribution of centromeres visualised by p35S::tdTomato-CENH3 in interphase nuclei in the MZ and DZ. Nuclei were visualised using

pRPS5a::H2B-GFP. The images are shown as maximum z-projections. Bars = 5 μm. b, Quantitative analysis of the degree of bias in centromere distribution in interphase nuclei in the MZ. First, the longitudinal axis (blue dotted line) was determined by drawing a line through the centres of neighbouring nuclei in the cell file. Next, the transverse axis (green dotted line) was drawn perpendicular to the longitudinal axis in the centre of the target nucleus, dividing it into two equal hemispheres. Then, the number of centromeres (magenta circles) in each hemisphere was counted and divided by 10, the maximum number of centromeres. Between the two values obtained in each nucleus, the higher value was adopted as the biased level. As the lowest value is 0.5, the value minus 0.5 is shown. The graph shows the average ± S.E. n = 23, $p < 0.001$ by Student's t-test. c, Dynamics of centromeres visualised by p35S::CENH3-tdTomato from metaphase to early G1 phase. Nuclei are visualised in green by pRPS5a::H2B-GFP. The images are shown as maximum z-projections. Bars = 5 μm.

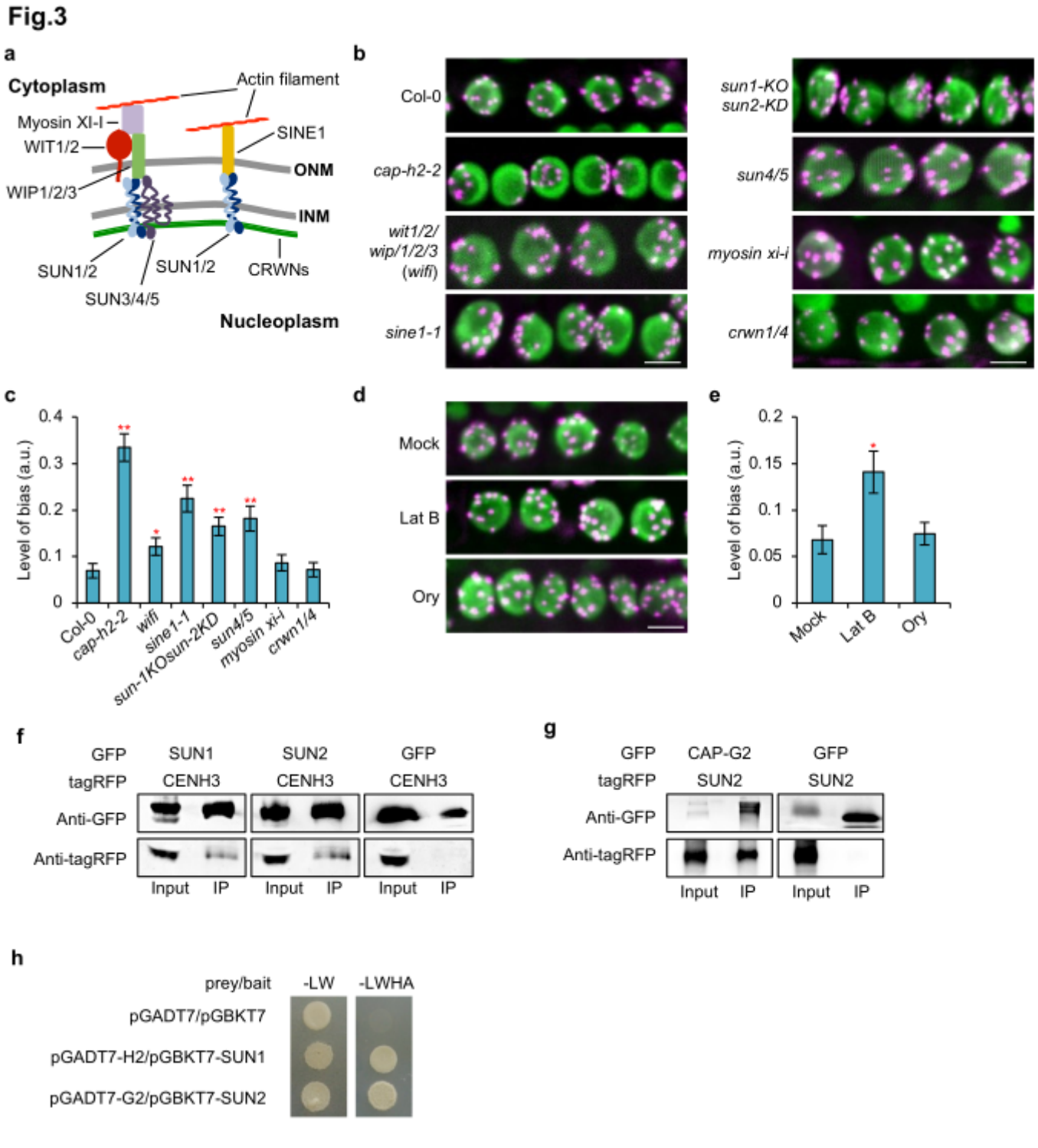

Figure 3

LINC complexes are involved in the formation of scattered centromere distribution in cooperation with condensin II a, Two different LINC complexes spanning the outer (OMN) and inner (INM) nuclear membranes. b-e, Analysis of centromere distribution in mutants defective in (b,c) proteins of the LINC complex or after disrupting (d,e) actin filament or microtubule dynamics by latrunculin B (Lat B) or oryzalin (Ory) treatment. b,d, Fluorescent images of centromeres visualised by p35S::tdTomato-CENH3 (magenta) in interphase nuclei of the MZ. Nuclei were visualised using pRPS5a::H2B-GFP (green). The

images are shown as maximum z-projections. Bars = 5 μm. c,e, Quantitative analysis of bias in centromere distribution in interphase nuclei of the MZ. The graph shows the average ± S.E. n > 21, *p < 0.05, ** p < 0.01, Student's t-test. f, Co-IP assays of SUN proteins with CENH3. p35S::SUN1-GFP, p35S::SUN2-GFP, p35S::GFP, and p35S::CNEH3-tagRFP were infiltrated into N. benthamiana leaves. Extracted proteins were immunoprecipitated with anti-GFP antibody and immunoblotted with anti-tagRFP antibody. g, Co-IP assay of SUN2 with CAP-G2. p35S::CAP-G2-GFP, p35S::GFP, and p35S::CNEH3-tagRFP were infiltrated into N. benthamiana leaves. Extracted proteins were immunoprecipitated with anti-GFP antibody and immunoblotted with anti-tagRFP antibody. h, Yeast two-hybrid assays of condensin II subunits CAP-H2 and GAP-G2 with SUN proteins. Yeast transformants were dropped onto SD/-Leu/-Trp (-LW) and SD/-Leu/-Trp/-His/-Ala (-LWHA) media to assess protein–protein interactions.

Fig.4

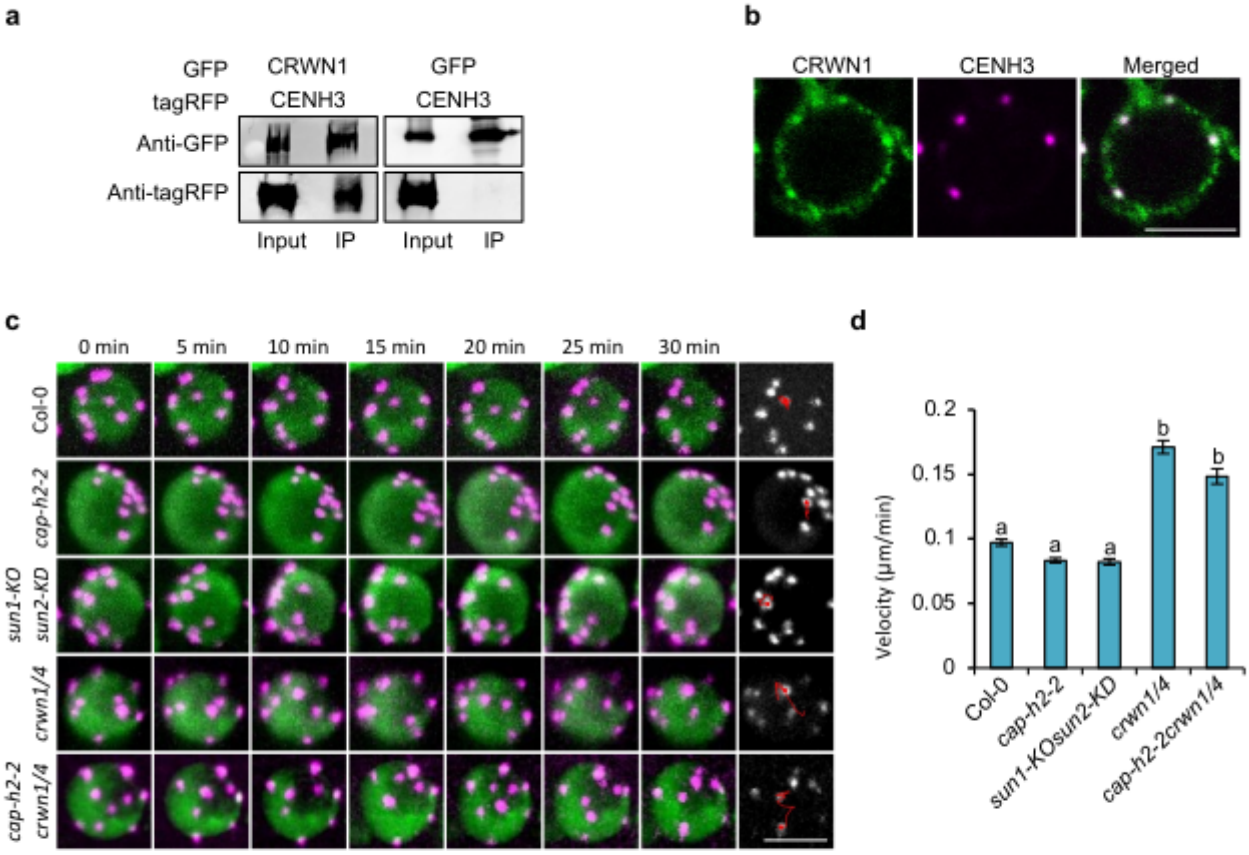

Figure 4

CRWNs stabilize centromere position during interphase a, Co-IP assay of CRWN1 with CNEH3. p35S::CRWN1-GFP and p35S::CENH3-tagRFP were infiltrated into N. benthamiana leaves. Extracted proteins were immunoprecipitated with anti-GFP antibody and immunoblotted with anti-tagRFP antibody. b, Simultaneous observation of CRWN1 in green and CENH3 in magenta visualised by p35S::CRWN1-GFP and p35S::CENH3-tdTomato, respectively, in interphase nuclei of the MZ. The images are shown as maximum z-projections. Bar = 5 μm. c, Centromere dynamics visualised by p35S::tdTomato-CENH3

(magenta) during interphase in nuclei of the MZ (5 min intervals). Nuclei were visualised using pRPS5a::H2B-GFP (green). The images are shown as maximum z-projections. The rightmost panel shows the trajectory of a centromere's movement over 30 min (yellow line). Bar = 5 μm. d, Quantitative analysis of centromere movement in interphase nuclei of the MZ. The velocity of centromere movement was calculated using the images shown in (a). The graph shows the average ± S.E. n > 49, p < 0.01, by one-way ANOVA and Tukey's HSD.

Fig.5

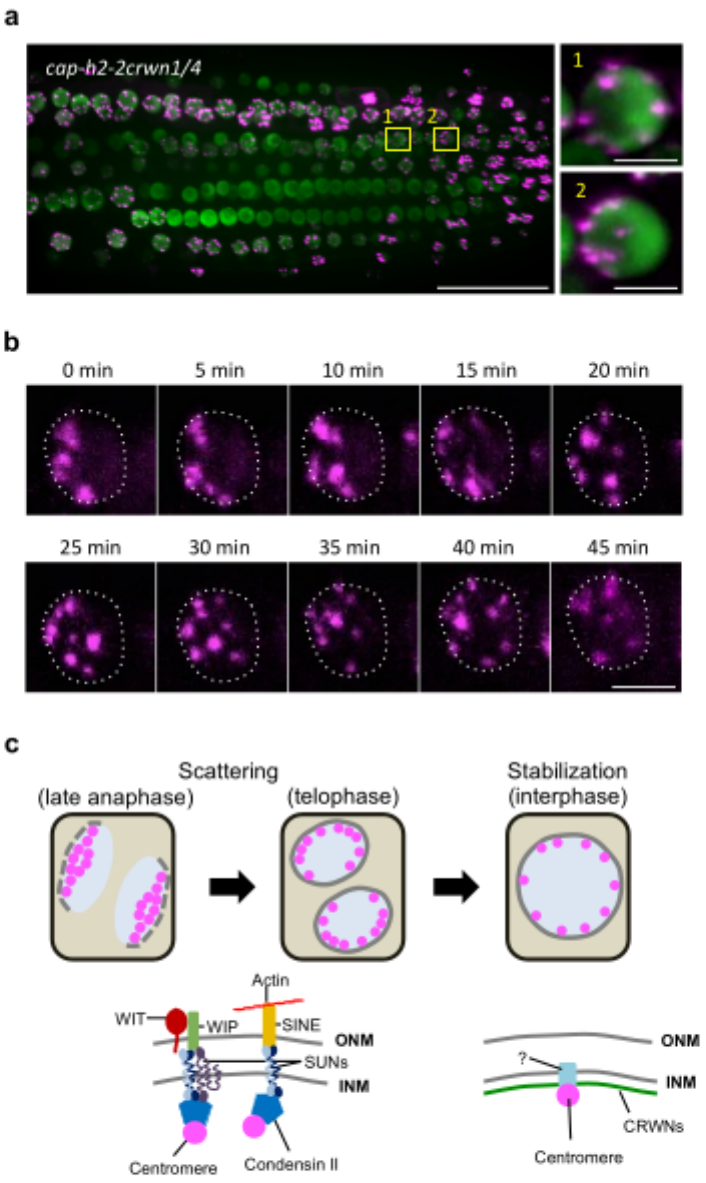

Figure 5

CII-LINC and CRWNs independently contribute to the regulation of centromere distribution a Centromere distribution visualised by p35S::tdTomato-CENH3 (magenta) in the root of a cap-h2-2crwn1/4 mutant. The right panels show magnified images of the nuclei in the yellow boxes in the left panel. Nuclei were visualised using pRPS5a::H2B-GFP (green). Bars = 50 μm and 5 μm in left and right panels, respectively. b, Dynamics of centromeres visualised by p35S::tdTomato-CENH3 (magenta) in the cap-h2-2crwn1/4 triple mutant. The outline of nuclei is indicated by white dotted lines. The images are shown as maximum z-projections. Bar = 5 μm. c, Schematic model of the two-step process regulating centromere distribution over the mitotic cell cycle.

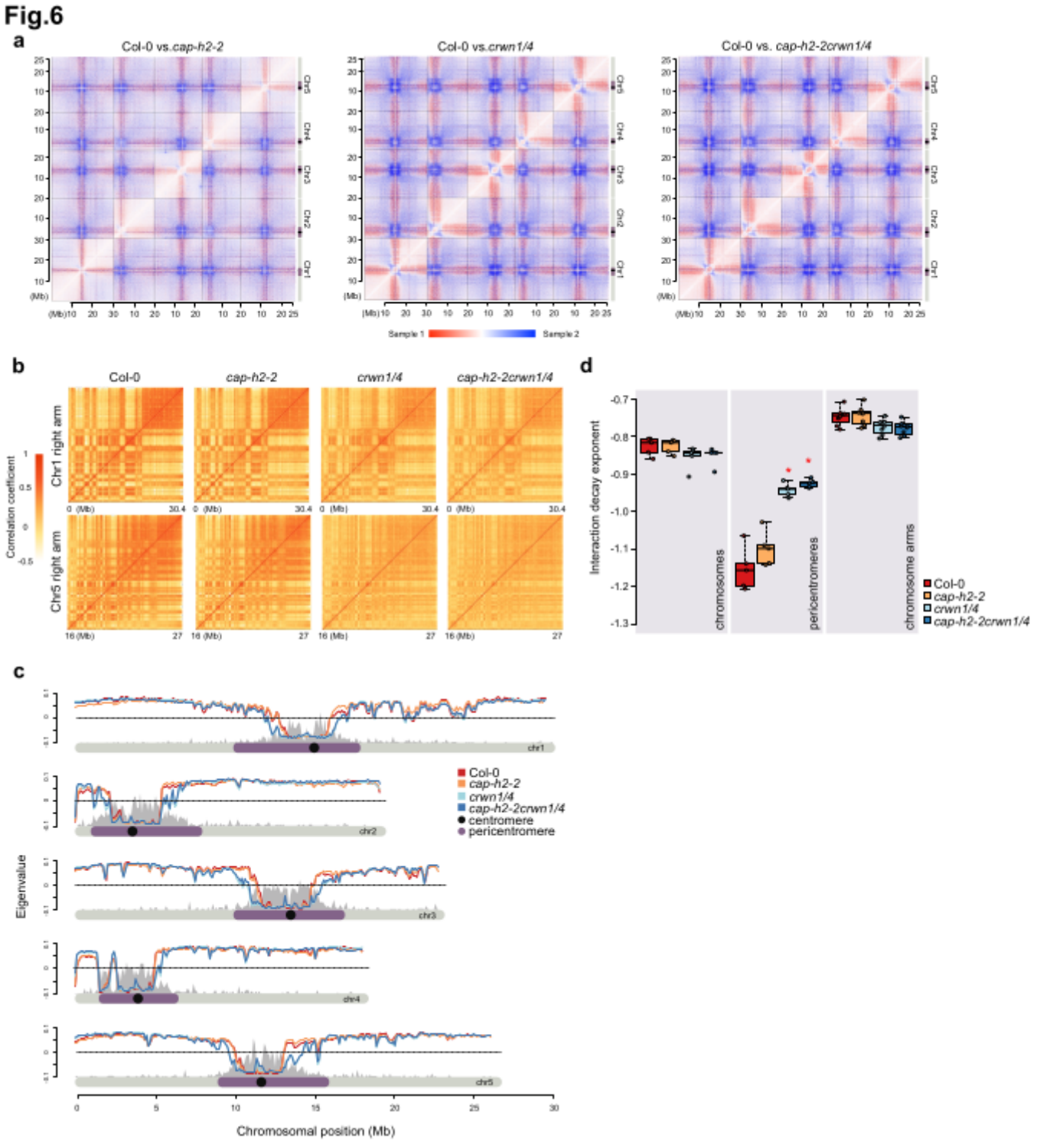

Figure 6

Comparison of chromatin organization between the wild type and the mutants of condensin II and CRWNs a, Enrichment of interaction frequencies obtained by calculating the relative difference between two interactomes of the indicated lines. b, Distance-normalised correlation matrices of Hi-C contact maps of chromosome 1 right and chromosome 5 right arms for the indicated lines. c, Distribution of eigenvectors for each entire chromosome in indicated lines. The grey peaks indicate the distribution of transposons. d, Distribution of IDEs of the full genomes, pericentromeres, and chromosome arms for the indicated lines. $p < 0.001$ by Student's t-test. a-d, bin size; 50 kb.

Fig.7

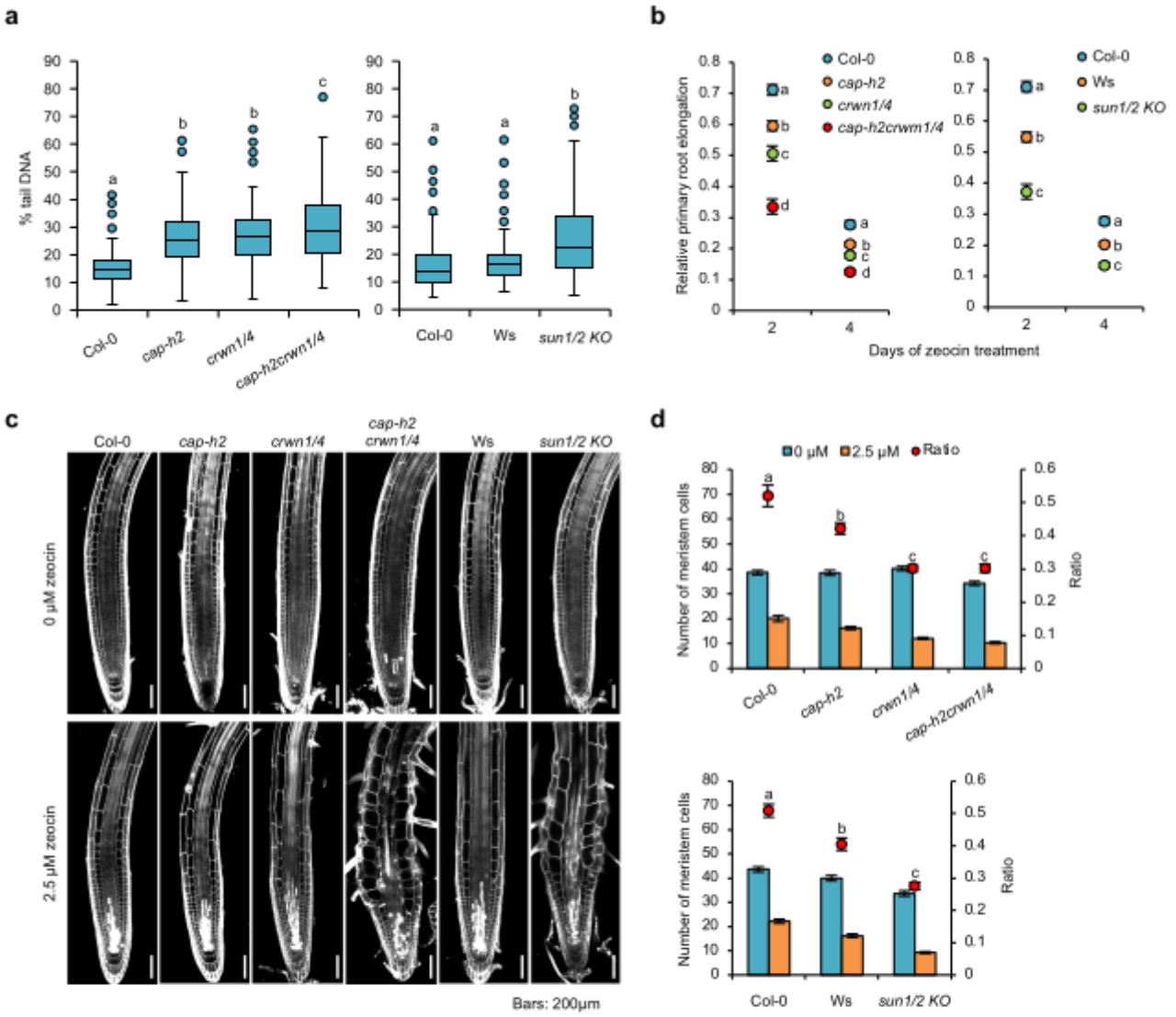

Figure 7

Factors required for the regulation centromere distribution are involved in the maintenance of genome integrity a, Quantitative analysis of DSBs in the root tips of the indicated lines. At least 118 nuclei were observed in each treatment group. The first and third quartiles with the median are shown boxes with cross bars, lower and upper whiskers represent the entire range of data points, dots indicate outliers. $n > 117$, $p < 0.05$, one-way ANOVA and Tukey's HSD. b, Sensitivity of primary root growth to the DSB-inducing reagent zeocin (5 μM). Values are ratios relative to the values under normal conditions. The graph shows the average ± S.E. $n > 18$, $p < 0.05$, by one-way ANOVA and Tukey's HSD. c, Effect of zeocin treatment on root tips. The roots were stained with PI. Fluorescent images of root tips treated with 0 or 2.5 μM zeocin for 2 days are shown. Bars = 200 μm. d, Effect of zeocin treatment on root meristem size. The number of meristematic cortex cells was counted using images shown in (c). Values are ratios relative to the values under normal conditions. The graph shows the average ± S.E. $n > 26$, $p < 0.05$, by one-way ANOVA and Tukey's HSD.

Supplementary Files

This is a list of supplementary files associated with this preprint. Click to download.

- SupplementaryFigures.pptx
- 210808SupplementaryTableS1.xlsx
- 210808SupplementaryTableS2.xlsx
- SupplementalData1.xlsx
- SupplementalData2.xlsx